Numerical simulation of fatigue crack propagation in WC-Co hardmetal

Utku Ahmet Özden, Keng Jiang, Alexander Bezold, Christoph Broeckmann
Institute for Materials Applications in Mechanical Engineering (IWM) RWTH Aachen University,
Augustinerbach 4, 52062, Aachen, Germany
Tel: +492418099537, u.oezden@iwm.rwth-aachen.de

Jose María Tarragó, Alvaro Mestra, Luis Llanes
Departament de Ciència dels Materials i Enginyeria Metallúrgica (CIEFMA), ETSEIB, Universitat
Politècnica de Catalunya, Avda. Diagonal 647, 08028, Barcelona, Spain

ABSTRACT

WC-Co cemented carbides (hardmetals) are a group of composite materials exhibiting outstanding combinations of hardness and toughness. As a consequence, they are extensively used for highly demanding applications, such as cutting and drilling tools, where cyclic loading is one of the most critical service conditions.

A numerical study of the mesoscale fatigue crack growth in WC-Co is here conducted. Within this context, a model based on a continuum damage mechanics approach was implemented in commercial solver Abaqus/Explicit for simulating the crack propagation in the material. Separate damage laws, based on brittle failure and fatigue, were used for describing the mechanical response of WC and Co phases, respectively. Material parameters for the carbide phase were taken from literature, whereas those for the metallic phase were experimentally determined in a model binder-like Co-base alloy, i.e. one with a composition representative of the binder phase within a commercial hardmetal grade.

In order to validate the approach used, a numerical model based on a real damaged microstructure was generated. It is found that proposed model is capable of capturing damage evolution with cyclic loading in WC-Co, as numerical results reflect satisfactory agreement with real crack pattern resulting from experiments.

KEYWORDS

WC-Co; Hardmetals; Finite Element Method (FEM); Continuum Damage Mechanics (CDM); Fatigue; Crack propagation; Microstructure.

INTRODUCTION

WC-Co cemented carbides, also referred to as hardmetals, are one of the most widely used composite materials because of their exceptional combination of hardness, strength and wear resistance. Main reason behind it is the quite different, but complementary, mechanical properties exhibited by their two interpenetrating phases: a hard, brittle (elastic) ceramic phase (WC) and a soft, ductile (elasto-plastic) metallic one (Co). Strength degradation of cemented carbides under cyclic loads is a phenomenon known since the early 1940s [1]. Since then, extensive and systematic research conducted by different groups worldwide has allowed to establish that hardmetals are fatigue-sensitive [2]. In general, a tradeoff between monotonic (fracture strength

and toughness) and cyclic (fatigue strength and crack growth resistance) properties is discerned with increasing binder content and carbide grain size, pointing out the compromising role of the ductile binder as the toughening- and fatigue-susceptible agent in these materials. However, to the best knowledge of the authors, most of the work published regarding fatigue of these materials has mainly concentrated in experimental approaches (e.g. Refs. [3-6]). On the other hand, although some numerical studies dealing with microcrack initiation and propagation in WC-Co materials are found in open literature, they are completely limited to mechanical response under monotonic loading [7,8].

Following the above ideas, it is the main focus of the present study to simulate the mesoscale crack propagation in WC-Co under cyclic loads, using finite element (FE) method. In this study, a model based on a continuum damage mechanics (CDM) approach, together with an element elimination based simulation technique, was used to describe the crack propagation in the material. In this regard, brittle and ductile damage laws were implemented for WC and Co phases respectively. The material parameters for WC are taken from literature. Meanwhile, the material parameters for the metallic phase are experimentally determined from the mechanical response exhibited by a model binder-like alloy. It permits to identify parameters for defining accurate plasticity and damage models in the metallic phase. Details of these works are provided elsewhere [9]. Finally, aiming to validate the developed approach, a numerical model based on a real damaged microstructure is generated, and the results of the two studies are compared.

1. EXPERIMENTAL WORK

In order to conduct fatigue crack growth (FCG) experiments, hardmetal samples specific for the current study were produced. A material containing a relatively high carbide content was preferred for industrial relevance. Accordingly, an experimental grade, referred to as "E10", was produced by Ceratizit S.A. Basic microstructural, physical and mechanical characteristics for the material studied are listed in Table 1.

Table 1. Basic microstructural, physical and mechanical characteristics of the E10 grade.

	WC wt. %	WC vol. %	Vickers Hardness (HV)	WC grain size μm	Elastic Modulus - E (GPa)	Poisson's ratio - ν	Density (g/cm^3)
E10	89.9	83.5	1190	2.09	582.3	0.224	14.5

FCG samples were produced such that chemical composition of the binder within the composite was as close as possible to that exhibited by the referred model binder-like alloy [9]. They were then machined and ground into prismatic specimens having dimensions of 45x10x5 mm. Longitudinal surfaces were polished up to mirror-like finish, in order to avoid residual stresses induced by previous grinding stages. Samples were then single-edge notched (SENB) by electrical discharge machining. It was followed by notch tip sharpening using a razor blade impregnated with diamond paste. The resulting notches had dimension of ~2 mm length with a tip curvature of ~8 μm (Fig.1).

In order to nucleate a sharp crack out of the notch tip, cyclic compressive loads were first applied on the specimens by means of a standard four point bending setup. Stable crack growth was observed during cyclic compression, with nucleated cracks being arrested after an extension of ~30 μm. However, it is already known from literature that, after cyclic compressive loading, residual tensile stresses might occur in the vicinity of the notch due to the cyclic plasticity during unloading

from the maximum compression [10]. This was overcome by further propagation of the microcracks, under cyclic tensile loading, such that they could be extended far from the region close to notch tip [11]. This was done by imposing a stress intensity range just above to the expected threshold one, about 7.2 MPa.m$^{1/2}$ for a hardmetal microstructure similar to the one exhibited by E10 specimen [11], to avoid unstable crack extension. FCG rate measurements were divided into certain number of steps with respect to number of cycles. After each step, crack length was measured and the max/min applied loads were recalculated in order to maintain a constant ΔK. Microcracks were propagated during 50,000 cycles. Image sequence of the above-mentioned process: notching, crack nucleation and stable crack growth in the near threshold regime is shown in Fig.2. A series of samples were successfully cracked, and growth behavior of these microcracks was used for implementing the numerical simulation procedure.
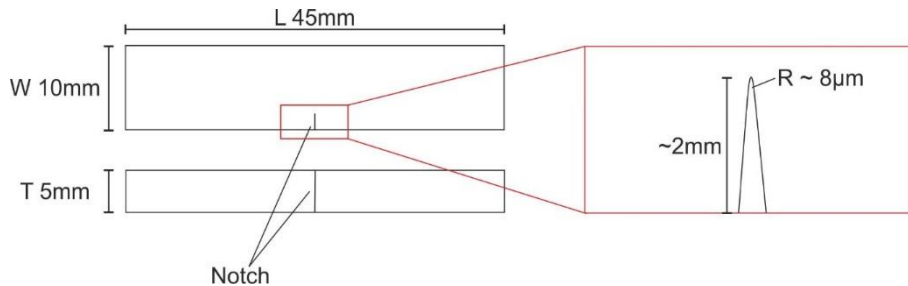

Fig.1. Schematic representation of the E10 test specimen.

Since specimens were through-thickness notched, microcrack formation was observed on both sides of the specimen. Based on detailed SEM imagery, microcrack profile of the sample on both sides was obtained. Microcracks of 226 and 433 µm, running on front and back surfaces of the sample, were recorded. Crack paths in the SEM mosaics are highlighted Fig.3.

As observed from the images, microcracks follow almost a linear pattern, without any branching. However, a detailed inspection indicates that there exist several breaks in the cracks paths. There are a couple of possible explanations for such finding. First, samples were placed in the SEM chamber right after the experiment, without any further surface treatment. Therefore, it is quite a challenge to track the crack path within the binder phase, since the crack pattern mainly diminishes in the background. Second, there is a strong possibility that in-between breaks, crack path is still continuous, but below the surface. Furthermore, since the intensity of the breaks increases mainly at the end of the path, it is possible that crack paths at those regions were not fully developed, resulting then in partial crack patterns. Nevertheless, for each case it was possible to track uninterrupted microcrack patterns, feasible enough for direct comparison with findings from the numerical studies.

Although the microcracks were observed on both surfaces, only the microcracks running on one side of the specimens were selected for the simulation. Cleanness of the notch region and the microcrack profile for the numerical modelling was the major criteria for the selection. In this regard, the back surface of the sample was selected for the simulations.
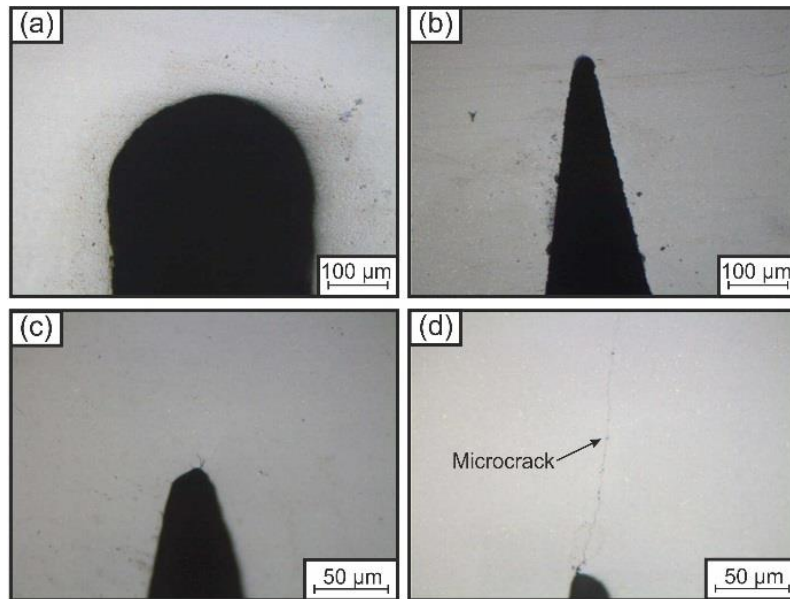
Fig.2 Fatigue precracking of E10 notched specimen, (a) notch generation by EDM (~200 µm), (b) sharpening of the notch by the razor blade (~8 µm), (c) nucleation of the microcracks under cyclic compression (reverse bending), and (d) propagation of the microcrack under cyclic tension (tensile bending).
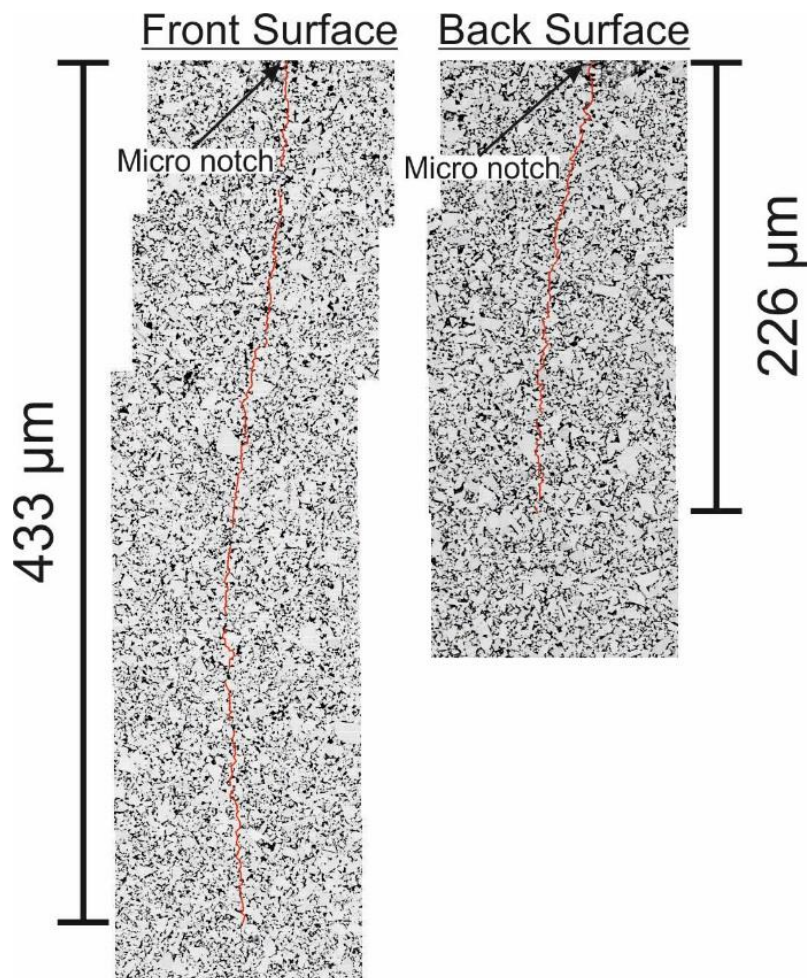

Fig.3 Microcracks observed on the front and back surfaces near the notch region for the experimental specimen ($\Delta K = 7.2$ MPa.m$^{1/2}$, N = 50,000).

2. NUMERICAL METHODOLOGY

Both phases of the material were modeled based on a CDM approach with quite distinct damage laws. Based on this approach, elements are either degraded or removed from the model as soon as certain damage criteria are met, and both lead to a degradation of global stiffness. Similar techniques have also been applied by other researchers [12]. Implementation of this technique required material models for both phases to be developed as user defined material subroutine (VUMAT) in the commercial software Abaqus 6.12 [13]. Solutions were then calculated in the FEM solver Abaqus using an explicit scheme, in order to overcome numerical divergence problems.

A relatively simple damage law based on the maximum principal stress (σ_I) was recalled for the brittle carbide phase. The corresponding linear elastic constitutive equation is defined by generalized Hooke's law:

$$\boldsymbol{\sigma} = \boldsymbol{C}^{el} : \boldsymbol{\varepsilon} \tag{1}$$

where $\boldsymbol{\sigma}$, $\boldsymbol{\varepsilon}$ and $\boldsymbol{C}^{el}$ are the second order stress tensor, strain tensor and fourth order elasticity tensor respectively, and σ_1 is defined in 2D plane stress as:

$$\sigma_1 = \frac{(\sigma_{xx}+\sigma_{yy})}{2} + \sqrt{(\frac{\sigma_{xx}-\sigma_{yy}}{2})^2 + \sigma_{xy}{}^2} \tag{2}$$

where σ_{xx}, σ_{yy}, σ_{xy} are the normal and shear components of the stress tensor. Based on the above law, within the subroutine damage for the WC grain is triggered as soon as the critical failure stress value is achieved ($\sigma_1 \geq \sigma_{1c}$). Thus, the element is eliminated from the global stiffness matrix in the next sequential step.

Material properties such as the elastic modulus (E) and poison's ratio (ν) for the WC were derived from literature. However, to the best knowledge of authors, an exact value of the maximum critical strength for a single carbide grain is not available in open literature. Moreover, it is known that tungsten carbide crystals are highly anisotropic [14]. WC-Co composites with very high carbide content (90-95 wt. % WC) may reach transverse rupture strength values up to 4000 MPa [15]. Therefore, being the most relevant, this value was adopted as an averaged single value for the maximum critical principal stress (σ_{1c}) for the WC phase. Material parameters for this ceramic phase, to be later used for the simulation, are given in Table 2.

Regarding the metallic binder, a non-linear damage law based on accumulated plastic strain was defined. In CDM, formulation of the constitutive equations for strain and damage characterizes the plain material itself, without any volume or surface discontinuity. Hence, the damage parameter D can be defined as the surface density of microcracks and microvoids when only isotropic damage is considered:

$$D = \frac{\delta S_D}{\delta S} \tag{3}$$

where δS_D and δS are the damaged and total surface areas respectively. Thus, considering a homogenized response within a single element, the "effective stress" is defined as the stress acting on the resisting area, i.e. $\delta \bar{S} = \delta S - \delta S_D$.

In the case of isotropic damage under uniaxial loading, without the closure effect of microcracks in compression, the mean value of the microstresses is simply given by the force equilibrium as [16]:

$$\widetilde{\sigma} = \frac{\sigma}{(1-D)} \tag{4}$$

where D is the scalar damage parameter, and σ and $\tilde{\sigma}$ are the actual and effective stresses respectively. The effective yield function based on a non-linear combined hardening law is defined as:

$$\tilde{f} = (\tilde{\boldsymbol{\sigma}} - \boldsymbol{\alpha})_{eq} - R - \sigma_y \tag{5}$$

where $\boldsymbol{\alpha}$, σ_y, R are the back stress, the yield strength and the isotropic hardening stress respectively. Evolution of $\boldsymbol{\alpha}$ with plastic strain (ε_p) may be described by a function including the hardening modulus c, the dynamic rate of backstress γ and the plastic strain itself, according to [17]:

$$\boldsymbol{\alpha} = \frac{c}{\gamma}(1 - e^{-\gamma\varepsilon_p}) \tag{6}$$

Considering a material subjected to J_2 flow theory, thus (5) can be explicitly written as:

$$F(\tilde{\boldsymbol{\sigma}} - \boldsymbol{\alpha}) = \sqrt{\frac{3}{2}\left(\tilde{\sigma}_{ij}^D - \alpha_{ij}^D\right)\left(\tilde{\sigma}_{ij}^D - \alpha_{ij}^D\right)} - R - \sigma_y \tag{7}$$

In this equation, $\tilde{\sigma}_{ij}^D$ and α_{ij}^D are the deviatoric part of the effective and backstress tensors, and the associated plastic flow is given by:

$$\dot{\boldsymbol{\varepsilon}} = \dot{\boldsymbol{\varepsilon}}_e + \dot{\boldsymbol{\varepsilon}}_p \tag{8}$$

$$\dot{\boldsymbol{\varepsilon}}_p = \frac{\partial F}{\partial \boldsymbol{\sigma}}\dot{\varepsilon}_{eq}^{pl} \tag{9}$$

$$\dot{\varepsilon}_{eq}^{pl} = \sqrt{\frac{2}{3}\dot{\boldsymbol{\varepsilon}}_p : \dot{\boldsymbol{\varepsilon}}_p} \tag{10}$$

where $\dot{\boldsymbol{\varepsilon}}$, $\dot{\boldsymbol{\varepsilon}}_e$, $\dot{\boldsymbol{\varepsilon}}_p$ are the total, elastic and accumulated plastic strain rates, and $\dot{\varepsilon}_{eq}^{pl}$ is the equivalent (accumulated) plastic stain rate, respectively. The full damage constitutive equation for the Co phase is derived from [18], and defined in the user subroutine as follows:

$$\dot{D} = \begin{cases} \left(\frac{\Gamma}{H}\right)^h \dot{\varepsilon}_{eq}^{pl}, & if \ \varepsilon_{eq}^{pl} > 0 \\ 0, & if \ not \end{cases} \tag{11}$$

where

$$\begin{cases} \Gamma = \frac{\tilde{\sigma}_{eq}^2 R_v}{2E} \\ R_v = \frac{2}{3}(1 + v) + 3(1 - 2v)\left(\frac{\sigma_H}{\sigma_{eq}}\right)^2 \end{cases} \tag{12}$$

being Γ the energy density release rate, R_v the triaxiality function, E the elastic modulus, v the Poisson's ratio, σ_H the hydrostatic stress and σ_{eq} the equivalent stress. Here the variables h and H are two material parameters which depend on temperature. Since temperature has no effect on the current study, both parameters were set to unit values. Similar to the case for the carbide phase, damage for the metallic one is triggered as soon as the critical damage parameter is achieved ($D \geq D_c$), resulting in the elimination of the element from the global stiffness matrix in the next sequential step.

Material properties for the Co phase, required for the simulation, were mainly derived from the experiments conducted with the referred representative binder alloy [9]. Various test specimens were produced from the alloy and material parameters such as the elastic modulus (E), yield stress

(σ_y), hardening modulus (C), and the dynamic rate of the backstress (γ) were determined from standard tensile and cyclic load experiments. The value for the Poison's ratio (v) and the critical damage parameter (D_c) were taken from literature (Table 2).

Table 2. Material properties for the WC and Co phases.

Material	E (GPa)	v (-)	σ_y (MPa)	C (GPa)	γ (-)	D_c	σ_{1c} (MPa)
WC	700[19]	0.24[19]	-	-	-	-	4000
Co	227.28	0.3[19]	683.07	52.38	151.64	0.3[18]	-

3. MULTISCALE SIMULATION

For the numerical simulation, a multiscale approach was preferred. In this regard, initially the FCG specimen (macroscale) was simulated analogue to the experimental setup. In order to simulate fatigue crack evolution, a certain section of the specimen's microstructure (mesoscale) was modelled. Dimensions of this section were chosen based on the computational capacity and robustness of the model. The link between the two scales was conducted by a simplified sub-modelling approach. Since the original orientation of the microcrack surface is already known, the global stresses derived from a single critical element were mapped over the later generated microstructure model. By doing so, a direct link between macro- and meso-scales was generated. The implementation of the selected approach is described below.

A macroscopic numerical model was initially generated. It was done on the basis of the experimental E10 specimen (see Fig.1) and testing conditions. In high cycle fatigue experiments, samples are submitted to very low external loads and the stress caused by these loads do not exceed the macroscopic yield limit at any material point. Therefore, plasticity was neglected for the model, and the linear elastic material parameters (E and v) for the WC-Co were used (Table 1). The model was simplified based on the symmetric nature of the sample and the test setup. The resulting model was composed of 286,225 first order linear elastic hexahedral elements (Fig.4)
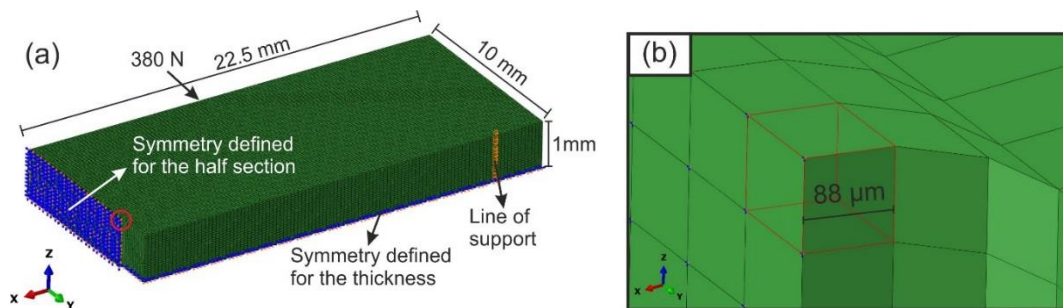

Fig.4 FE model based on the SENB specimen, (a) standard four-point bending configuration, (b) critical hexahedral element for calculating the global stresses.

A single static solution was conducted for the maximum and minimum loads applied on the specimen. Since the applied load over the specimen was cycled with a constant load ratio of 0.1, only the maximum applied load of 1520 N (380 N due to quarter model) was applied on the macroscopic model. As expected, the stress state from the hexahedral element located on the edge of the micronotch was observed to be critical (Fig.4b). Therefore, assuming a stress state unified over the single element, the stress tensor components for this single element were extracted. However, in order to decrease the excessive computational demand, a 2D plane stress simplification was used for the microstructural model. It is known that plane stress elements are suitable for simulating surface cracks [20]; thus, only the surface microstructure of the sample was modeled. Based on the orientation of the 2D surface over the hexahedral element, only the global stress components acting over the surface ($\Sigma_{xx}, \Sigma_{xy}, \Sigma_{yy}$) were mapped to the microstructural model. From the single integration point of the critical element, values of 437.3 MPa, 114.4 MPa and 97.9 MPa were calculated for the $\Sigma_{xx}, \Sigma_{xy}, \Sigma_{yy}$ respectively.

For the modelling of the microstructural model, sections of the SEM images were used. Considering numerical efficiency and complications in model generation, the model was limited to a size of 65x65 µm. The average element size used was calculated to be 0.3 µm for optimum performance; hence, microscopic details below this threshold value were omitted. However, in some critical regions (especially where crack propagation was observed) such details were kept by local enrichment in the mesh. The existing microcrack was deleted from the model, and the microscopic forces derived from the global stress components were applied over the two edges of the model. In order to initiate the microcrack in the correct position, a few elements were deleted to create an initial crack of ~2.5 µm. For the conversion of the global stress components to the microscopic forces, a unit thickness for the model was assumed. For the other edges of the model, simple symmetric boundary conditions were defined (Fig.5). Similar to the experimental testing conditions, cyclic loading was defined as following a constant sinusoidal frequency and under a load ratio of R = 0.1. The predefined material properties were applied for the WC and Co phases (Table 2).
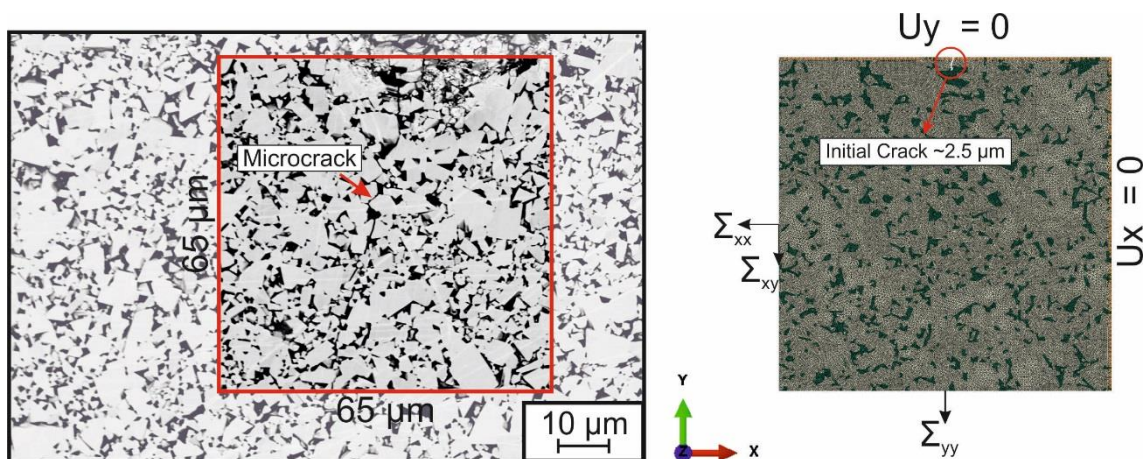

Fig.5 Microstructural FE model and the corresponding boundary conditions, based on the SEM images near the notch region.

4. RESULTS AND DISCUSSION

Based on the simulation results, cyclic evolution of the microcrack was successfully observed within the microstructural model. It is shown in Fig. 6 as a series of sequential images. The microcrack propagates in a stable manner, from the initially defined crack position, up to 330 cycles. As the crack reaches a carbide boundary, the stress level ahead of the crack tip is required to be higher than the defined damage criterion (σ_{1c}) to observed rapid crack propagation through

the WC phase. This extension generally occurs in a single cycle, as expected from the perfectly brittle material definition implemented for the WC phase. On the other hand, as the crack reaches the Co phase, its propagation is controlled by the cyclic accumulation of plastic strain. Further stable crack propagation combined with sudden jumps as the crack meets and overcomes a carbide boundary finally lead to unstable crack growth (Fig. 7). As highlighted before, recent observations in literature indicate degradation (or even inhibition) of toughening mechanism for the Co phase as the driving force for subcritical FCG in hardmetals [6], and this is also captured by the model.
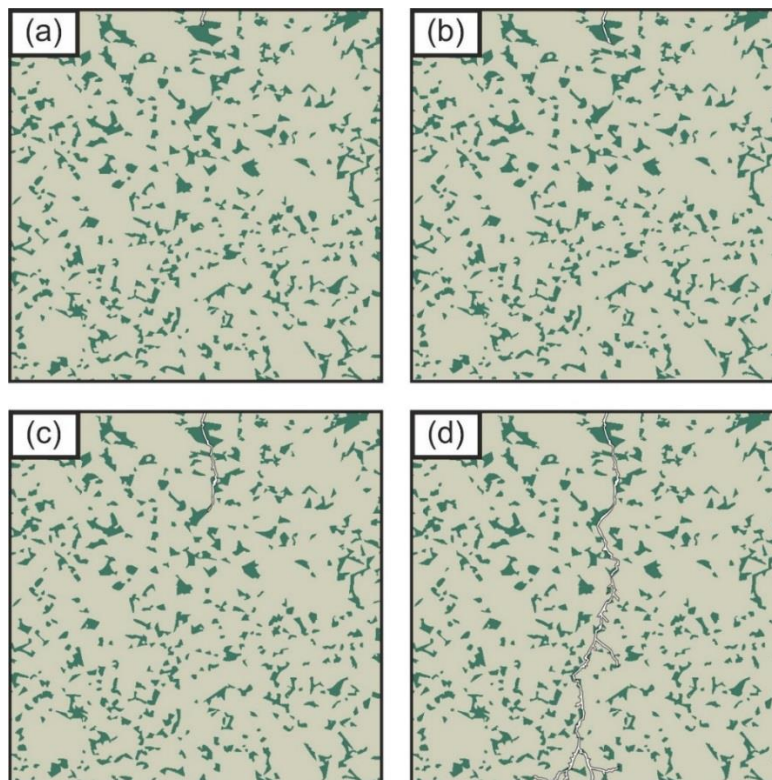

Fig.6 Evolution of damage in the microstructural model at (a) 0 cycles, (b) 300 cycles, (c) 330 cycles, (d) 332 cycles.

The range of the stable crack growth in the model is relatively shorter than the one experimentally discerned. Although it was initially attributed to the overall dimensions of the mode, later studies indicated that size of the model has minimum influence within the stable crack propagation regime. Hence, the observed discrepancy could be rationalized on the basis that assumption done on the brittle response for the WC phase may not correctly reflect the physical nature of this material. In this regard, it is known that certain amount of plastic deformation is also evidenced within the WC particles [21]. This might delay the propagation of the crack during fatigue. Furthermore, it should be recalled that load control was applied during the experiment in order to guarantee stable growth of the crack up to a certain length. However, such a control over the load was not conducted for the numerical simulation, since the model is relatively small in dimensions. Implementation of load control conditions within larger models, in order to increase the range of stable crack growth, is considered as further research actions.

A comparison between the real and the simulated crack patterns is provided in Fig. 8. For the sake of clarity, both crack paths are highlighted on the real microstructure. The results of the simulation reflect excellent agreement with the experimental findings in the short/stable crack growth region. A relatively fair agreement is observed for the unstable crack growth part. However, it has to be indicated that the number of cycles to failure should not be considered in a quantitative manner, since those values are strongly affected by the element size and the overall size of the model.

Nevertheless, it may be pointed out that model does qualitatively capture a fracture pattern similar to that observed in a real cyclic loading experiment.
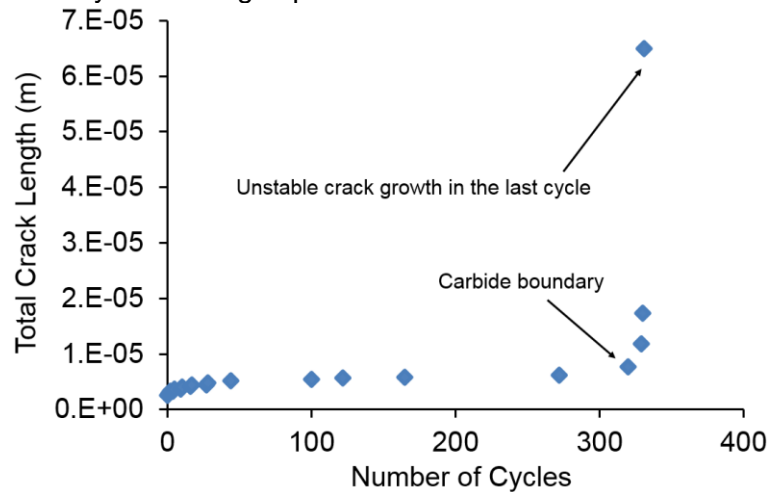

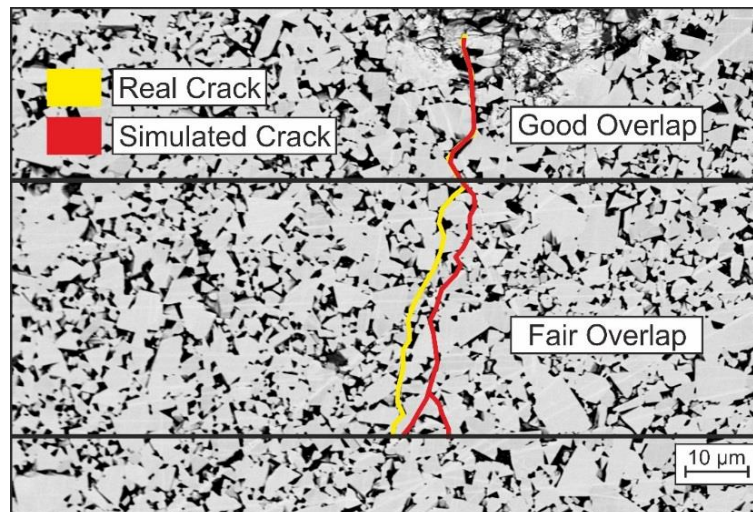Fig.7 Evolution of the total crack length with respect to number of cycles.

Fig.8 Comparison between the real and simulated crack patterns and various zones of crack propagation.

5. CONCLUSION

In this study, a numerical model based on results obtained from real experimental tests was generated. Main goal behind it was to simulate the microstructural evolution of a fatigue crack in a WC-Co hardmetal. In this regard, a finite element model based on a continuum damage mechanics approach was implemented in commercial solver Abaqus/Explicit for simulating crack extension in the material. Separate damage laws, based on brittle failure and fatigue, are implemented for the WC and the Co phases respectively.

Although a small section of the experimental model was considered, the model is found to be capable of capturing the cyclic evolution of the simulated crack pattern. Moreover, satisfactory agreement between the real and the simulated crack paths were observed.
For the sake of simplicity and computational efficiency, the model excludes many other physical aspects of the fatigue phenomena within WC-Co materials. However, even it is somehow simplified the model was able to capture a realistic fatigue crack propagation behavior for the material studied. In this regard, the model is considered to be valid for conducting comparative studies

based on artificial microstructures. This will be quite useful for evaluating the influence of different microstructural parameters on the FCG performance of hardmetals.

ACKNOWLEDGEMENTS

REFERENCES

[1] Dawihl, W, 1941, Die wissenschaftlichen und technischen grundlagen der pulvermetallurgie, stahl und Eisen, 61, 909-919.

[2] Llanes, L, Anglada, M, Torres, Y, 2014, Fatigue of cemented carbides, Comprehensive Hard Materials, Elsevier, Vol. 1, 345-362.

[3] Schleinkofer, U, Sockel, HG, Görting, K, Heinrich, W, 1997, Fatigue of hard metals and cermets - new results and a better understanding, Int J Refract Met H, 15, 103-112.

[4] Sailer, T, Herr, M, Sockel, HG, Schulte, R, Feld, H, Prakash, LJ, 2001, Microstructure and mechanical properties of ultrafine-grained hardmetals, Int J Refract Met H, 19, 553-559.

[5] Kursawe, S, Pott, Ph Sockel, HG, Heinrich, W, Wolf, M, 2001, On the influence of binder content and binder composition on the mechanical properties of hardmetals, Int J Refract Met H, 19, 335-340.

[6] Tarrago, JM, Jimenez-Pique, E, Turon, M, Rivero, L, Schneider, L, Llanes, L, 2013, Toughening and fatigue micromechanisms in hardmetals: FESEM/FIB tomography characterization, 18th Plansee Seminar, Reutte, paper #HM54.

[7] Fischmeister, HF, Schmauder, S, Sigl LS, 1988, Finite element modelling of crack propagation in WC-Co hard metals, Mater Sci Eng A, 105-106, 305-311.

[8] McHugh, PE, Connolly, PJ, 2003, Micromechanical modelling of ductile crack growth in the binder phase of WC–Co, Comput Mater Sci, 27, 423-436.

[9] Özden, UA, Mingard, KP, Zivcec, M, Bezold, A, Broeckmann, C, 2015, Mesoscopical finite element simulation of fatigue crack propagation in WC/Co-hardmetal, Int J Refract Met H, 49, 261-267.

[10] Godse, R, Gurland, J, Suresh, S, 1988, Effects of residual stresses in fracture toughness testing of hard metals. Mater Sci Eng A, 106, 383-387.

[11] Llanes, L, Torres, Y, Anglada, M, 2002, On the fatigue crack growth behavior of WC-Co cemented carbides: kinetics description, microstructural effects and fatigue sensitivity, Acta Mater., 50, 2381-2393.

[12] Mishnaevsky Jr., L, Dong, M, Hönle, S, Schmauder, S, 1999, Computational mesomechanics of particle-reinforced composites, Comput Mater Sci, 16, 133-143.

[13] Abaqus 6.12, 2013, Abaqus user subroutines reference manual.

[14] Exner, HE, Gurland, J, 1970, A Review of parameters influencing some mechanical properties of tungsten carbide-cobalt alloys. Powder Metall, 13, 13-31.

[15] General Carbide, 2009, The Designer's Guide to Tungsten Carbide, Greensburg.

[16] Rabotnov, YN, 1968, Creep rupture, 12th International Congress of Applied Mechanics, Stanford, California, 342-349.

[17] Dunne, F, Petrinic, N, 2005, Introduction to computational plasticity, Oxford University Press.

[18] Lemaitre, J, Desmorat, R, 2005, Engineering damage mechanics, Springer-Verlag.

[19] Sadowski, T, Nowicki, T, 2008, Numerical investigation of local mechanical properties of WC/Co composite, Comput Mater Sci, 43, 235-241.

[20] Schmauder, S, 2001, Crack growth in multiphase materials, Encyclopedia of Materials: Science and Technology, Pergamon.

[21] Exner, HE, 1979, Physical and chemical nature of cemented carbides, Int Mater Rev, 24, 149-173.